

# Dynamical friction on binary stars in dark matter dominated environments

Nicolas Esser\*

*Service de Physique Théorique, Université libre de Bruxelles and  
Brussels Laboratory of the Universe – BLU-ULB  
Boulevard du Triomphe, CP225, 1050 Brussels, Belgium*

(Dated: February 25, 2026)

We study binary stars moving through a uniform dark matter background and experiencing dynamical friction. The centre-of-mass motion of the pairs is taken into account. We derive formulas and timescales for the secular evolution of the orbital parameters for both wide and close binaries. We apply these results to environments typical of dark matter dominated ultra-faint dwarf galaxies and show that some binaries undergo significant eccentricity oscillations, while their semi-major axes decrease more gradually. We consider a simple binary star population and find that dynamical friction, notably, can enhance the bias from unresolved binaries in velocity dispersion measurements. With future, more detailed theoretical studies and improving observational capabilities, binary stars may serve as a tool to probe the dark matter content of some of the faintest galaxies.

## I. INTRODUCTION

The nature of dark matter (DM) remains one of the most pressing questions in astrophysics [1]. While multiple observations indicate its presence on galactic and extragalactic scales, probing DM on subgalactic scales is challenging. Nevertheless, such investigations could provide significant insights into its fundamental properties [2].

Here, we explore the effect of dark matter on binary stellar systems. DM in the form of massive compact objects would inject energy into binaries, possibly leading to their disruption [3]. In contrast, if DM consists of objects lighter than stars, it would instead exert dynamical friction on them, thereby altering their orbital evolution and producing potentially observable signatures. However, the effect of DM friction on binaries in the solar neighborhood was studied decades ago and found to be negligible [4].

But the discovery of tens of DM-dominated ultra-faint dwarf galaxies (UFDs) around the Milky Way over the past two decades has opened a new testbed for dark matter [5]. Thanks to ever-improving observational capabilities, progressively fainter systems continue to be discovered each year [6, 7], and significant progress has recently been made in detecting and characterizing binaries within these galaxies [8–11]. This raises the question of the impact of DM dynamical friction on binary stars in such environments.

In this paper, we characterize the long-term secular evolution of binary orbital parameters induced by DM dynamical friction. After introducing the general framework for dynamical friction acting on binary stars in Sec. II, we analyze two opposite regimes. In Sec. III, we consider wide binaries, whose orbital velocities are small compared to their centre-of-mass (CoM) velocities. The opposite regime, corresponding to close binaries, is

treated in Sec. IV. We derive analytical expressions and timescales for both regimes and apply them, in Sec. V, to a simple binary star population in an environment typical of UFDs. We conclude in Sec. VI.

Our results indicate that binary stars can be significantly affected by dynamical friction in dense UFDs. In particular, this effect may enhance biases in velocity dispersion measurements, and thus in estimates of the DM content of such systems. Ultimately, binaries themselves could serve as a probe of dark matter in some of the faintest galaxies.

## II. DYNAMICAL FRICTION ON BINARIES

We use the Chandrasekhar formula to describe the dynamical friction exerted on a star of mass  $m_i$  moving with velocity  $\mathbf{v}_i$  through a DM background of uniform density  $\rho_{\text{dm}}$ . Assuming that the DM particles follow a Maxwellian velocity distribution with dispersion  $\sigma$ , the acceleration due to dynamical friction reads [12, 13],

$$\mathbf{f}_i = -4\pi G^2 \rho_{\text{dm}} m_i \ln \Lambda \mathcal{A}\left(\frac{v_i}{\sigma}\right) \frac{\mathbf{v}_i}{v_i^3}, \quad (1)$$

with  $\mathcal{A}(X)$  a dimensionless monotonic function, described in Appendix A, such that  $\mathcal{A}(X \rightarrow 0) \propto X^3$  and  $\mathcal{A}(X \rightarrow \infty) = 1$ . One therefore recovers the standard results  $f_i \propto v_i^{-2}$  for  $v_i \gg \sigma$  and  $f_i \propto v_i$  for  $v_i \ll \sigma$ . The Coulomb logarithm  $\ln \Lambda$  has been assigned various expressions in the literature [13, 14]. We follow [13] and adopt  $\ln \Lambda = \ln [r_{1/2} v_i^2 / (G m_i)] = 10$  for the remainder of this work. This value is appropriate for stars moving at a few km/s in ultra-faint dwarf galaxies with typical half-light radii  $r_{1/2} \sim \mathcal{O}(10)$  pc. Because of the logarithm, even strong variations in the above parameters lead only to  $\mathcal{O}(1)$  changes. The dynamical friction acceleration arises from the gravitational force generated by the wake of DM particles trailing a star as it moves through the background. The mass of this wake is proportional to the stellar mass; more massive stars generate larger wakes, which in turn slow them down more

\* nicolas.esser@ulb.be

effectively. Consequently, the strength of the dynamical friction acceleration scales with  $m_i$ .

In a binary stellar system, the velocity of each component can be decomposed as  $\mathbf{v}_i = \mathbf{v}_{\text{cm}} + \mathbf{v}_{\text{rel},i}$ , where  $\mathbf{v}_{\text{cm}}$  is the centre-of-mass velocity of the pair, and  $\mathbf{v}_{\text{rel},i}$  is the relative velocity of star  $i$  with respect to the CoM. The latter can be written as  $\mathbf{v}_{\text{rel},1} = \dot{\mathbf{x}}m_2/M$  and  $\mathbf{v}_{\text{rel},2} = -\dot{\mathbf{x}}m_1/M$ , with  $M = m_1 + m_2$  the total mass of the system, and  $\dot{\mathbf{x}}$  the relative velocity between the two stars, whose separation vector  $\mathbf{x}$  points from the second star to the first. Using Eq. (1), the effect of dynamical friction on the global motion of the pair follows from the definition of the CoM velocity,  $\mathbf{f}_{\text{cm}} = (m_1\mathbf{f}_1 + m_2\mathbf{f}_2)/M$ , while its effect on the internal orbital motion is  $\mathbf{f}_{\text{df}} = \mathbf{f}_1 - \mathbf{f}_2$ , that is,

$$\mathbf{f}_{\text{df}} = -4\pi G^2 \rho_{\text{dm}} \ln \Lambda \times \left[ m_1 \mathcal{A} \left( \frac{v_1}{\sigma} \right) \frac{\mathbf{v}_1}{v_1^3} - m_2 \mathcal{A} \left( \frac{v_2}{\sigma} \right) \frac{\mathbf{v}_2}{v_2^3} \right]. \quad (2)$$

The total internal acceleration of the system is given by  $\ddot{\mathbf{x}} = \ddot{\mathbf{x}}_0 + \mathbf{f}_{\text{df}}$ , where  $\ddot{\mathbf{x}}_0 = -GM\mathbf{x}/x^3$  is the standard two-body gravitational acceleration. The internal energy and angular momentum are defined as  $E = \mu(\dot{\mathbf{x}}^2/2 - GM/x)$  and  $\mathbf{L} = \mu\mathbf{x} \times \dot{\mathbf{x}}$ , from which one can derive their evolution under dynamical friction,

$$\dot{E} = \mu\dot{\mathbf{x}} \cdot \mathbf{f}_{\text{df}} \text{ and } \dot{\mathbf{L}} = \mu\mathbf{x} \times \mathbf{f}_{\text{df}}, \quad (3)$$

where  $\mu = m_1 m_2 / M$  is the reduced mass. The dynamical friction force is very weak compared to the mutual gravitational attraction of the binary components. Its effect therefore operates on a timescale much longer than the orbital period. As a result, a single orbit is effectively Keplerian. One can then write  $E = -GM\mu/(2a)$  and  $L = \mu\sqrt{GMa(1-e^2)}$ , with  $a$  and  $e$  the orbital semi-major axis and eccentricity of the reduced orbit. Because the evolution is slow, we are interested in the long-term, secular changes of the orbital parameters  $E$  and  $\mathbf{L}$ . Since a single orbit remains Keplerian, the orbital average of any quantity  $Q$  can be computed by integrating over the period, expressed in terms of the true anomaly  $\theta$ , via the relation (see e.g. [15])

$$\langle Q \rangle = \frac{(1-e^2)^{3/2}}{2\pi} \int_0^{2\pi} \frac{Q(\theta)}{(1+e\cos\theta)^2} d\theta. \quad (4)$$

We will use the orbit-averaged evolution of the orbital parameters to characterize the long-term behavior of binary systems.

Two simple cases will be considered: wide and close binaries, defined here as systems whose internal orbital velocity is small or large, respectively, compared to their CoM velocity. The transition between these two regimes occurs for binaries with typical separation

$$a \sim GM/v_{\text{cm}}^2 \sim 100 \text{ AU} \left( \frac{M}{M_{\odot}} \right) \left( \frac{3 \text{ km/s}}{v_{\text{cm}}} \right)^2. \quad (5)$$

### III. WIDE BINARIES

The wider the binary, the smaller the orbital velocity. In the limit where  $\dot{\mathbf{x}} \ll v_{\text{cm}}$ , expanding Eq. (2) at first order leads to

$$\mathbf{f}_{\text{df}} = - \frac{4\pi G^2 \rho_{\text{dm}} \ln \Lambda}{v_{\text{cm}}^3} \left[ (m_1 - m_2) \mathcal{A} \left( \frac{v_{\text{cm}}}{\sigma} \right) \mathbf{v}_{\text{cm}} + 2\mu \left( \mathcal{A} \left( \frac{v_{\text{cm}}}{\sigma} \right) \dot{\mathbf{x}} - \mathcal{B} \left( \frac{v_{\text{cm}}}{\sigma} \right) \frac{\dot{\mathbf{x}} \cdot \mathbf{v}_{\text{cm}}}{v_{\text{cm}}^2} \mathbf{v}_{\text{cm}} \right) \right], \quad (6)$$

where  $\mathcal{B}(X)$  is a dimensionless monotonic function, described in Appendix A, such that  $\mathcal{B}(X \rightarrow 0) \propto X^5$  and  $\mathcal{B}(X \rightarrow \infty) = 1$ . As is clear from Eq. (6), in this limit the orbital evolution due to dynamical friction depends on the relative orientation between the CoM velocity  $\mathbf{v}_{\text{cm}}$  and the orbital velocity  $\dot{\mathbf{x}}$ . We therefore need a fully general description of the Keplerian orbits, taking into account the orientation of the ellipse in three-dimensional space. This is usually done by writing  $\mathbf{x} = r \mathbf{u}_r$  with

$$r = \frac{a(1-e^2)}{1+e\cos\theta} \quad (7)$$

$$\mathbf{u}_r = \begin{bmatrix} \cos\Omega \cos(\omega+\theta) - \cos i \sin\Omega \sin(\omega+\theta) \\ \sin\Omega \cos(\omega+\theta) + \cos i \cos\Omega \sin(\omega+\theta) \\ \sin i \sin(\omega+\theta) \end{bmatrix},$$

where  $\theta$  is the true anomaly describing the time-dependent position of the stars,  $i$  is the inclination of the orbital plane with respect to the  $xy$ -plane,  $\Omega$  is the longitude of the ascending node, and  $\omega$  is the argument of periastris (see e.g. [16, 17]). The velocity  $\dot{\mathbf{x}}$  can be computed from Eq. (7) using  $d/dt = \dot{\theta} \cdot d/d\theta$ , with  $\dot{\theta} = L/(\mu r^2)$ .

With the help of Eqs. (3) to (7), one may evaluate  $\langle \dot{E} \rangle$ . Importantly, the zeroth-order part (i.e. the first line) of Eq. (6) depends only on the CoM velocity, and not on the orbital position or velocity. Once incorporated into the expression for  $\dot{E}$  and orbit-averaged, it therefore leads to a term proportional to  $\langle \dot{\mathbf{x}} \rangle = 0$ . The latter vanishes because the orbital velocity is large at small orbital radii, where the stars spend less time, and small at large radii, where they spend more time. When averaged over time, these contributions exactly cancel. The energy evolution is therefore dominated by the first-order corrections. Without loss of generality, we choose the CoM velocity to be oriented along the positive  $z$ -axis. One then finds

$$\langle \dot{E} \rangle = \frac{E}{\tau_{w,1}} \left[ 1 - \frac{\mathcal{B}(v_{\text{cm}}/\sigma)}{\mathcal{A}(v_{\text{cm}}/\sigma)} \frac{\sin^2 i}{2} (1 - \mathcal{F}(e) \cos 2\omega) \right] \quad (8)$$

where we have defined the wide binary energy loss (i.e. first order) timescale as

$$\tau_{w,1} = \left[ \frac{16\pi G^2 \rho_{\text{dm}} \mu \ln \Lambda}{v_{\text{cm}}^3} \mathcal{A} \left( \frac{v_{\text{cm}}}{\sigma} \right) \right]^{-1} \quad (9)$$

$$\sim 5 \times 10^9 \text{ yr} \left( \frac{100 \text{ GeV/cm}^3}{\rho_{\text{dm}}} \right) \left( \frac{\max(v_{\text{cm}}, \sigma)}{3 \text{ km/s}} \right)^3.$$

The numerical estimate assumes  $m_1 = m_2 = M_\odot$ , and the appearance of  $\max(v_{\text{cm}}, \sigma)$  arises from considering the two limiting regimes of  $\mathcal{A}(v_{\text{cm}}/\sigma)$ .  $\mathcal{F}(e)$  is a dimensionless monotonic function, described in Appendix A, such that  $\mathcal{F}(0) = 0$  and  $\mathcal{F}(1) = 1$ . The bracketed factor in Eq. (8) can take values  $\in [-2, 1]$ .

The evolution of the semi-major axis can be readily derived from its relation to the orbital energy,  $\dot{a} = -a\dot{E}/E$ , and can be either negative or positive. However, situations in which  $a$  increases are rare, as they typically require a peculiar combination of a CoM velocity larger than the velocity dispersion, a large eccentricity, and specific values of  $i$  and  $\omega$ , such that the bracketed factor in Eq. (8) becomes negative. For  $i = 0$  (a binary orbit perpendicular to the CoM velocity), one finds

$$a(t) = a_0 \exp(-t/\tau_{w,1}), \quad (10)$$

where  $a_0$  denotes the initial semi-major axis. Since  $\tau_{w,1}$  is independent of  $a_0$ , the ratio  $a(t)/a_0$  is also independent of  $a_0$ , thus implying a scale-invariant behaviour.

To fully characterize the evolution of the binary orbit, one must determine  $\dot{\mathbf{L}}$  in addition to  $\dot{E}$ . This, however, is still insufficient; an ellipse has five degrees of freedom: two specifying the orbital plane, one its overall size, one its eccentricity, and one the orientation of its major and minor axes within the plane. Energy and angular momentum account for only four of these. The remaining degree of freedom, associated with the orientation of the axes, is therefore undetermined. This ambiguity is commonly resolved by introducing the eccentricity (or Laplace-Runge-Lenz) vector. Alternatively, the orbit can be parametrized by the set  $\{a, e, i, \Omega, \omega\}$ , which is often more convenient. In particular, the evolution of these elements under an external perturbation has already been derived in the literature (see e.g. [16, 17]). While an orbit average can always be performed, it is particularly simple when the perturbation is constant – as is the case here at zeroth order in Eq. (6) – yielding

$$\begin{cases} \langle \dot{e} \rangle = -\frac{1}{\tau_{w,0}} \sqrt{\frac{a}{a_0}} \sqrt{1-e^2} \cos \omega \sin i \\ \langle \dot{i} \rangle = \frac{1}{\tau_{w,0}} \sqrt{\frac{a}{a_0}} \frac{e}{\sqrt{1-e^2}} \cos \omega \cos i \\ \langle \dot{\Omega} \rangle = \frac{1}{\tau_{w,0}} \sqrt{\frac{a}{a_0}} \frac{e}{\sqrt{1-e^2}} \frac{\sin \omega}{\tan i} \\ \langle \dot{\omega} \rangle = \frac{1}{\tau_{w,0}} \sqrt{\frac{a}{a_0}} \frac{(1-2e^2 - \cos 2i)}{2\sqrt{1-e^2}} \frac{\sin \omega}{\sin i} \end{cases} \quad (11)$$

As expected,  $\langle \dot{a} \rangle = 0$  is also recovered at zeroth order. We again assumed that the CoM velocity is oriented along the positive  $z$ -axis. We have defined the zeroth-order

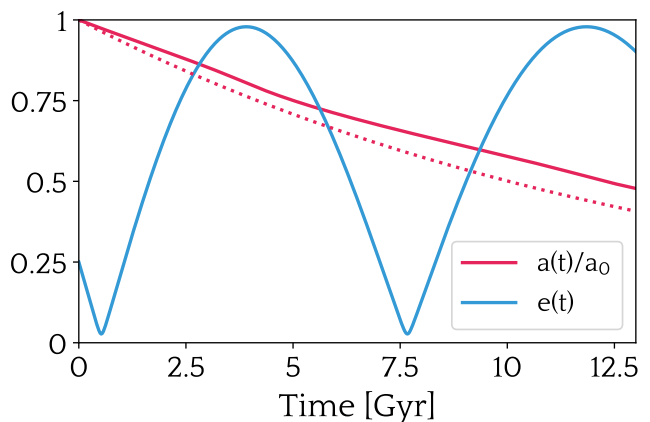


FIG. 1. Evolution of the semi-major axis (red) and eccentricity (blue) of a wide binary with  $m_1 = 1.5M_\odot$  and  $m_2 = 0.5M_\odot$ , initial values  $a_0 = 10^4$  AU and  $e_0 = 0.25$ , and CoM velocity  $v_{\text{cm}} = 3$  km/s, in an environment with  $\rho_{\text{dm}} = 100$  GeV/cm<sup>3</sup> and  $\sigma = 3$  km/s. Solid curves show the full evolution obtained by integrating Eqs. (8) and (11), while the dotted line shows the idealised analytical solution from Eq. (10). The orbital parameters  $i$ ,  $\Omega$ , and  $\omega$  also evolve but are not shown; changing their initial values leads to different evolutionary tracks.

wide binary evolution timescale as

$$\begin{aligned} \tau_{w,0} &= \left[ \frac{6\pi G^{3/2} \rho_{\text{dm}} (m_1 - m_2) \ln \Lambda \sqrt{a_0} \mathcal{A}\left(\frac{v_{\text{cm}}}{\sigma}\right)}{v_{\text{cm}}^2 \sqrt{M}} \right]^{-1} \\ &\sim 10^9 \text{ yr} \left( \frac{100 \text{ GeV/cm}^3}{\rho_{\text{dm}}} \right) \left( \frac{10^4 \text{ AU}}{a_0} \right)^{1/2} \\ &\quad \times \left( \frac{3 \text{ km/s}}{v_{\text{cm}}} \right) \left( \frac{\max(v_{\text{cm}}, \sigma)}{3 \text{ km/s}} \right)^3. \end{aligned} \quad (12)$$

The numerical estimate assumes  $m_1 = 1.5M_\odot$  and  $m_2 = 0.5M_\odot$ . Importantly,  $\tau_{w,0}$  is proportional to the mass difference between the two stars, and the evolution of  $\{e, i, \Omega, \omega\}$  is therefore slower when this difference is small. Moreover,  $\tau_{w,0} \propto \tau_{w,1} \sqrt{GM/a}/v_{\text{cm}}$ , indicating that the evolution of  $a$  is suppressed by one power of the velocity ratio relative to the other orbital parameters, as evident from the numerical estimates in Eqs. (9) and (12).

Figure 1 illustrates the evolution of  $a$  and  $e$  for a wide binary system in a DM-dominated, low-velocity-dispersion environment with  $\rho_{\text{dm}} = 100$  GeV/cm<sup>3</sup> and  $\sigma = 3$  km/s. Solid curves show the results of numerically solving Eqs. (8) and (11), while the dotted line corresponds to the idealised analytical solution from Eq. (10). As seen in the figure, binaries can undergo large eccentricity oscillations, while the semi-major axis changes only modestly over a Hubble time for the chosen environment properties. The eccentricity evolution arises from differential drag: both stars move through the same DM

background at nearly the CoM velocity, but since the dynamical friction acceleration depends on mass, the heavier star experiences a stronger drag, generating a torque on the pair that drives these oscillations. The semi-major axis evolves more slowly in the presence of CoM motion, because the stars are carried away from the DM wake they create, reducing the effective dynamical friction.

The reduction of the semi-major axis of wide binaries in dwarf galaxies has already been studied in Refs. [18, 19]. However, these works considered that the radius of the sphere of influence of each binary – corresponding to the typical size of the wakes generated in the DM background – was equal to the distance between the binary components, an assumption that is not generally valid. Focusing on circular orbits, they found an evolution timescale for  $a$  parametrically smaller than ours by a factor  $\propto \sqrt{GM/a}/\sigma$ , albeit with a larger numerical coefficient<sup>1</sup>. Overall, we find comparable values for the evolution timescale of  $a$  for very wide binaries with separations  $\sim 10^4$  AU. Moreover, our scaling agrees, up to a correction in the Coulomb logarithm, with the results of Refs. [20, 21] (see also [22]), which studied the effect of friction on binaries from first principles, without invoking the Chandrasekhar formula.

#### IV. CLOSE BINARIES

The Chandrasekhar formula encounters several problems for tight binaries. The typical size  $l$  of the DM wake generated by each star can be estimated by comparing the DM kinetic energy with the stellar gravitational potential, yielding  $l \sim Gm_i/\sigma^2$  [4]. For close binaries, the orbital velocity satisfies  $\dot{x} \sim \sqrt{GM/a} \gg v_{\text{cm}} \sim \sigma$ , implying  $a \lesssim l$ . In this regime, the wake generated by each star cannot be treated as affecting that star independently without also influencing its companion. Moreover, the energy extracted from the stars is transferred to the dark matter, which is heated and eventually ejected, leading over time to a depletion of the local DM background. While this effect is negligible when both the CoM velocity and the velocity dispersion greatly exceed the orbital velocity, it may become important in the opposite regime, where the stars can complete many orbits without significant motion through the galaxy and without sufficient time for dark matter to replenish the local environment.

While aware of these limitations, we will nonetheless employ the Chandrasekhar formula for tight binaries to obtain an estimate of the magnitude of its effects on such systems. The results presented below should therefore be regarded as idealized, and a more accurate treatment

will ultimately be required. Given the substantial effort needed to model the feedback of friction on the DM halo – even in simplified scenarios such as large mass-ratio binaries with negligible CoM motion [14] – we defer such a study to future work.

Close binaries have large orbital velocities. In the limit where  $\dot{x} \gg v_{\text{cm}}$ , the leading order of Eq. (2) is

$$\mathbf{f}_{\text{df}} = - \frac{4\pi G^2 M^3 \mu \rho_{\text{dm}} \ln \Lambda}{\dot{x}^3} \times \left[ \frac{1}{m_1^3} \mathcal{A} \left( \frac{m_1 \dot{x}}{M\sigma} \right) + \frac{1}{m_2^3} \mathcal{A} \left( \frac{m_2 \dot{x}}{M\sigma} \right) \right] \dot{\mathbf{x}}. \quad (13)$$

Since Eq. (13) depends only on the internal orbital velocity and not on the CoM velocity, the friction force is confined (at zeroth order) to the orbital plane, which therefore remains fixed in time. We can thus set  $\Omega = i = 0$ , i.e. take the orbital plane to coincide with the  $xy$ -plane. The direction of the angular momentum remains constant, and only its magnitude evolves in time. Given that the centre-of-mass velocity of a given binary is typically comparable to the velocity dispersion  $\sigma$ , one can further assume  $\dot{x} \gg \sigma$ , such that  $\mathcal{A}(m_i \dot{x}/(M\sigma)) \simeq 1$ . In this approximation, we can derive the evolution of  $E$  and  $L$  from Eqs. (3), (4) and (13) as

$$\begin{cases} \langle \dot{E} \rangle = \frac{E}{\tau_c} \left( \frac{a}{a_0} \right)^{3/2} \mathcal{K}(e, 1) \\ \langle \dot{L} \rangle = -\frac{L}{2\tau_c} \left( \frac{a}{a_0} \right)^{3/2} \mathcal{K}(e, 3), \end{cases} \quad (14)$$

with  $\mathcal{K}(e, n)$  a dimensionless monotonic function, described in Appendix A, such that  $K(0, n) = 1$ ,  $K(e \rightarrow 1, n) \rightarrow \infty$ , and  $\mathcal{K}(e, 3) > \mathcal{K}(e, 1)$ . We have defined the close binary evolution timescale as

$$\begin{aligned} \tau_c &= \left[ 8\pi \rho_{\text{dm}} \ln \Lambda \sqrt{GM}^{3/2} \mu \left( \frac{1}{m_1^3} + \frac{1}{m_2^3} \right) a_0^{3/2} \right]^{-1} \\ &\sim 10^{12} \text{ yr} \left( \frac{100 \text{ GeV/cm}^3}{\rho_{\text{dm}}} \right) \left( \frac{\text{AU}}{a_0} \right)^{3/2}, \end{aligned} \quad (15)$$

where the numerical estimate assumes  $m_1 = m_2 = M_\odot$ .

The evolution of the semi-major axis and the eccentricity can be straightforwardly derived from Eq. (14) using the relations  $\dot{a} = -a\dot{E}/E$  and  $\dot{e} = -(1 - e^2)/e \times [\dot{E}/(2E) + \dot{L}/L]$ . One finds in particular  $\langle \dot{a} \rangle = -a^{5/2} \mathcal{K}(e, 1)/(\tau_c a_0^{3/2})$ . In the case of circular orbits, i.e.  $e = 0$ , the solution for the semi-major axis as a function of time is

$$a(t) = a_0 (1 + 3t/2\tau_c)^{-2/3}. \quad (16)$$

Figure 2 shows the evolution of  $a$  and  $e$  for a close binary system in a DM-dominated, low-velocity-dispersion environment with  $\rho_{\text{dm}} = 10^4 \text{ GeV/cm}^3$  and  $\sigma = 5 \text{ km/s}$ .

<sup>1</sup> Note two typos in Ref. [18]. (i) The value given for their scaling factor is incorrect; the correct value is  $\alpha = 1.03$  [19]; and (ii) square roots are missing on the binary radii  $R_0$  in the expression for the time immediately below their Eq. (9).

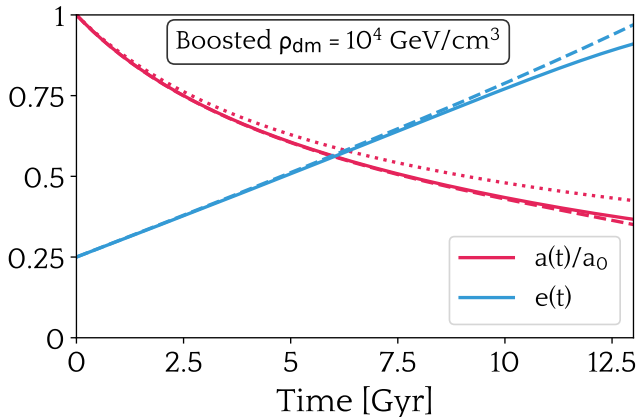


FIG. 2. Evolution of the semi-major axis (red) and eccentricity (blue) of a close binary of solar-mass stars with initial values  $a_0 = 1$  AU and  $e_0 = 0.25$ , in an environment with  $\rho_{\text{dm}} = 10^4$  GeV/cm<sup>3</sup> and  $\sigma = 5$  km/s. Solid curves show the result of numerically integrating Eq. (13), dashed curves correspond to the solution of Eq. (14), and the dotted curve shows the solution of Eq. (16).

Solid curves show the results of numerically integrating Eq. (13), without setting  $\mathcal{A}(X) = 1$ . Dashed curves correspond to the solution of Eq. (14) under the approximation  $\dot{x} \gg \sigma$ , and the dotted curve shows the analytical solution for circular orbits from Eq. (16). As one may read from the timescale (15), the DM density needs to be boosted to extremely high values, orders of magnitude beyond what is typically inferred in ultra-faint dwarf galaxies, for the effect of dynamical friction to be relevant in close binaries. In that case, we find that  $a$  decreases while  $e$  increases monotonically. The increase in eccentricity arises because the friction force, which scales as  $1/x^2$ , is stronger at apastron than at periastron [23, 24].

While the effect of DM friction on close binaries in the typical environments we consider is weak, we note that larger eccentricities lead to a stronger decrease in  $a$ , as seen in Eq. (14) and Fig. 2. In particular,  $\mathcal{K}(e, 1) \simeq 2$  for  $e = 0.9$  and  $\simeq 5$  for  $e = 0.999$ . This enhancement may cause some rare binaries – those that are relatively extended ( $\gtrsim 1$  AU) but have a slow CoM velocity, such that our approximation holds – to experience a non-negligible reduction of the semi-major axis in particularly dense UFD galaxies. However, this reasoning has limitations. At very high eccentricities, the velocity at apastron may become so small that the assumptions  $\dot{x} \gg v_{\text{cm}}$  and  $\dot{x} \gg \sigma$  break down, and the equations derived in this section are no longer applicable.

## V. EFFECT ON A STELLAR POPULATION

We consider, as a toy model, a population of binary stars with masses drawn from a Chabrier initial mass function [25], initial eccentricities following the thermal

distribution [26], and initial semi-major axes distributed according to a log-normal distribution [27]. Centre-of-mass velocities are drawn from a Maxwellian distribution with dispersion  $\sigma$ , and the relative orientation of the inner orbit with respect to the CoM velocity is picked at random. We only consider stars in the mass range  $[0.1, 0.8] M_{\odot}$ , as stars  $\gtrsim 0.8 M_{\odot}$  have reached the main-sequence turnoff in old stellar populations, while stars  $\lesssim 0.1 M_{\odot}$  are difficult to resolve individually in UFD galaxies at  $\mathcal{O}(10 - 100)$  kpc distances, even with ultra-deep James Webb Space Telescope photometry [9].

We take as example parameters those inferred from the recently discovered faint stellar system DELVE 1 [6, 28]. Conservative estimates of its line-of-sight velocity dispersion give an upper bound of  $\sigma_{\text{los}} = 1.2$  km/s, while its projected half-light radius is  $r_h = 6.2$  pc. Three-dimensional quantities are related by  $\sigma = \sqrt{3}\sigma_{\text{los}}$  and  $r_{1/2} = 4r_h/3$ . Using the mass estimator for dispersion-supported stellar systems from [29], the total mass within the half-light radius of DELVE 1 is given by  $M_{1/2} = 4G^{-1}\sigma_{\text{los}}^2 r_h \simeq 8300 M_{\odot}$ . If the system is dark matter dominated, as would be expected given its very low absolute V-band magnitude  $M_V = -0.2$  with respect to its inferred mass, this would imply a mean dark matter density of  $\rho_{\text{dm}} \simeq 133$  GeV/cm<sup>3</sup>. We note that, while DELVE 1 is not yet confirmed as a UFD, several systems – some of which have been confirmed as DM-dominated – share similar properties [5].

We numerically solve the general equation of binary evolution (Eq. (2)) for 1000 pairs, in an orbit-averaged manner (Eq. (4)). However, as a compromise between computational speed and accuracy, when the CoM velocity exceeds three times (or falls below one third of) the maximum (minimum) orbital velocity of the binary, we instead use the much more simple equations for wide (tight) binaries (Eqs. (8), (11) and (13)). We also verified that, in the appropriate limits, integrating the general equations reproduces the same results as these simplified expressions. Motivated by the old and relatively simple stellar populations of UFDs [5], we evolve all stars for 13 Gyr.

In Fig. 3, we show the distribution in initial (blue) and final (red) semi-major axis (left panel) and eccentricity (right panel) of the population. In particular, we observe an overall increase in the number of high-eccentricity pairs and a rise in the number of binaries with semi-major axes around  $\sim 10$  AU, accompanied by a corresponding decrease in the number of low-eccentricity and wide binaries. While these changes are relatively small, the effect is stronger for heavier stars, as shown in the inset plots, which include only binaries with total mass  $M > 0.8 M_{\odot}$ . There are 178 such binaries in the sample. In addition, the median orbital velocity of the  $M > 0.8 M_{\odot}$  population goes from  $\sim 5$  km/s to  $\sim 7.5$  km/s, increasing by roughly 50%. Because the DM content of faint stellar systems is inferred from velocity dispersion measurements of their more massive stars, an increased fraction of fast-orbiting binaries in this population would further amplify

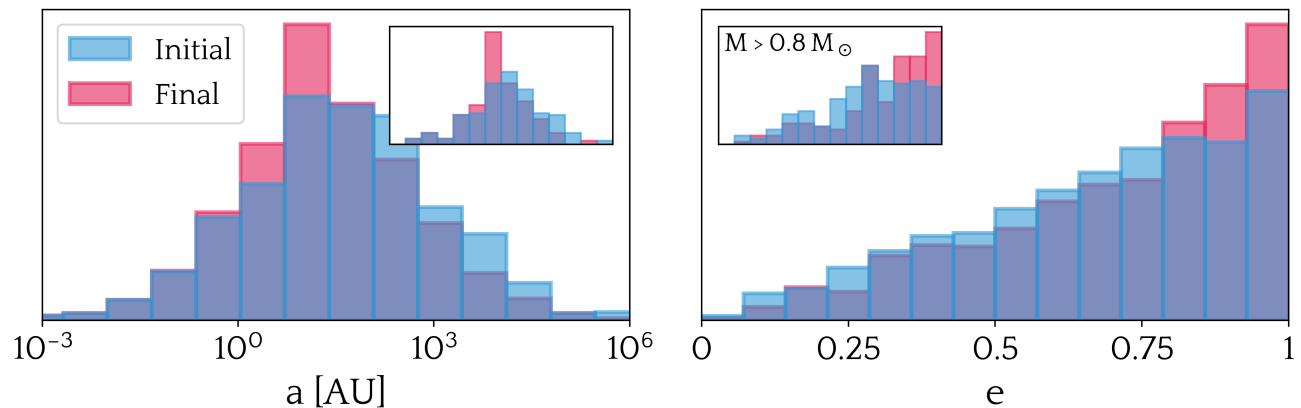


FIG. 3. Distribution of the initial (blue) and final (red) semi-major axes (left panel) and eccentricities (right panel) for a population of 1000 low-mass binaries evolved for 13 Gyr under dark matter dynamical friction, assuming  $\rho_{\text{dm}} = 133 \text{ GeV}$  and  $\sigma = 2.1 \text{ km/s}$ . The inset histograms highlight the 178 binaries with total mass  $M > 0.8 M_{\odot}$ .

the bias introduced by unresolved binaries, which tends to lead to an overestimation of the DM density in these systems [30–32].

Another interesting property is the increase in the number of binary systems with small periastron passages. For example, in the initial population, there are 259 pairs with periastron distances  $< 1 \text{ AU}$ . After evolving the population, and accounting for the combined effects of eccentricity oscillations in wide binaries and eccentricity growth in tight binaries, we find that over the age of the galaxy a total of 351 pairs experience passages below  $1 \text{ AU}$ . Approximately 10% of the binaries in the sample therefore reach sub-AU separations at some point due to dark matter friction. This may lead to tidal interactions, potentially inducing dynamical and chemical effects within the pair members.

## VI. CONCLUSION

We have studied in detail the effect of dark matter dynamical friction on binary stars, provided analytical formulas and timescales for the evolution of the orbital parameters, and applied these results to a simple population of binaries.

We found that, in environments typical of ultra-faint dwarf galaxies, wide binaries may undergo strong eccentricity oscillations on  $\sim \text{Gyr}$  timescales, while their semi-major axes evolve more gradually. For tight binaries, eccentricity tends to increase and semi-major axis decrease, although on a timescale much larger than the age of the Universe. This evolution typically leads to a larger fraction of high eccentricity systems and to an overall rise in the orbital velocities of the stellar population. It also results in more stars undergoing small periastron passages. Possible consequences of these effects are enhanced biases on velocity dispersion measurements and strengthened tidal interactions between the binary mem-

bers. More detailed theoretical studies will be needed to quantify these effects accurately.

Several improvements remain to be addressed in future work. First, the applicability of the Chandrasekhar formula to close binaries must be clarified, as the DM wakes generated by the individual stars cannot be treated independently in this regime. A key objective is therefore to characterize dynamical friction in such systems using dedicated simulations that account for overlapping wakes and feedback on the DM background [14]. Additional physical effects should also be incorporated to fully describe the dynamical evolution of binaries in UFDs, including galactic tides, three-body encounters, and migration toward the galactic centre driven by DM friction. In Appendix B, we estimate the associated timescales and find that galactic tidal forces may dominate for binaries with separations  $\gtrsim$  a few  $\times 10^3 \text{ AU}$ . A comprehensive numerical integration including all these processes is left for future work. Furthermore, the presence of specific DM and stellar density profile [33] and of a non-smooth DM component, such as massive subhalos [34, 35], may influence our results and warrant further investigation. Finally, adopting a more realistic initial distribution for the stellar population would provide a more complete and robust assessment.

While we applied our calculations to ultra-faint dwarf galaxies, other heavily DM-dominated systems include DM spikes that may form around supermassive black holes [36, 37]. In such spikes, the DM density can reach  $\gtrsim 10^6 \text{ GeV/cm}^3$ , although the velocity dispersion is higher than in UFDs. DM friction will influence binaries in these environments, but the tidal effects of the black hole cannot be neglected, requiring a coupled analysis of both phenomena. Nevertheless, these systems could produce interesting observable signatures in the binary population.

DELVE 1 was chosen as a representative system for our analysis, but many other faint stellar systems exist,

some of which have been confirmed to possess significant DM content. New faint systems are discovered every year, and their classification often requires multiple observations combining chemical and dynamical information. One such recently discovered object is the faint star cluster UNIONS 1 [38]. Although initially thought to be the most DM-dense galaxy ever identified [39], subsequent studies suggest that it likely does not contain a significant amount of DM [40] (but see also [41]). Rescaling our results to a system of this type – assuming it is DM-dominated – indicates that it should contain virtually no wide binaries, and that most of its close binaries should have large eccentricities. The identification and characterization of even a few binaries in such a system could therefore provide significant constraints on its dark matter.

Upcoming surveys and instruments will enable the dis-

covery of tens of new faint systems around the Milky Way (see e.g. [42–45]) and allow more precise measurements of the binaries they contain (see e.g. [46–48]). Together, these developments underscore the need for further theoretical studies of the dynamical evolution of stars in the faintest Milky Way satellites, as well as dedicated observational searches for binaries, which may provide valuable insight into their nature and dark matter content.

## ACKNOWLEDGMENTS

It is a pleasure to thank Peter Tinyakov for the many valuable discussions, and Marine Prunier for her helpful comments on the manuscript. The author is a FRIA grantee of the Fonds de la Recherche Scientifique-FNRS. Tag: ULB-TH/26-04

- 
- [1] M. Cirelli, A. Strumia, and J. Zupan, arXiv preprint , arXiv:2406.01705 (2024).
  - [2] J. Zavala and C. S. Frenk, *Galaxies* **7**, 81 (2019).
  - [3] M. A. Monroy-Rodríguez and C. Allen, *The Astrophysical Journal* **790**, 159 (2014).
  - [4] J. D. Bekenstein and R. Zamir, *The Astrophysical Journal* **359**, 427 (1990).
  - [5] J. D. Simon, *Annual Review of Astronomy and Astrophysics* **57**, 375415 (2019).
  - [6] S. Mau *et al.*, *The Astrophysical Journal* **890**, 136 (2020).
  - [7] C. Y. Tan *et al.*, arXiv preprint , arXiv:2510.11684 (2025).
  - [8] M. Safarzadeh, J. D. Simon, and A. Loeb, *The Astrophysical Journal* **930**, 54 (2022).
  - [9] C. Shariat *et al.*, *Publications of the Astronomical Society of the Pacific* **137**, 104103 (2025).
  - [10] F. Muratore *et al.*, arXiv preprint , arXiv:2512.01547 (2025).
  - [11] T. Qiu *et al.*, arXiv preprint , arXiv:2512.04477 (2025).
  - [12] S. Chandrasekhar, *The Astrophysical Journal* **97**, 255 (1943).
  - [13] J. Binney and S. Tremaine, *Galactic Dynamics: Second Edition* (Princeton University Press, 2008).
  - [14] B. J. Kavanagh, T. K. Karydas, G. Bertone, P. Di Cintio, and M. Pasquato, *Phys. Rev. D* **111**, 063071 (2025).
  - [15] M. Maggiore, *Gravitational Waves: Volume 1: Theory and Experiments* (Oxford University Press, 2007).
  - [16] E. Poisson and C. M. Will, *Gravity: Newtonian, Post-Newtonian, Relativistic* (Cambridge University Press, 2014).
  - [17] R. Bate, D. Mueller, and J. White, *Fundamentals of Astrodynamics* (Dover Publications, 1971).
  - [18] X. Hernandez and W. H. Lee, *Monthly Notices of the Royal Astronomical Society* **387**, 17271734 (2008).
  - [19] X. Hernandez and P. Kroupa, arXiv preprint , arXiv:2511.03776 (2025).
  - [20] A. Gould, *The Astrophysical Journal* **379**, 280 (1991).
  - [21] G. D. Quinlan, *New Astronomy* **1**, 3556 (1996).
  - [22] P. Pani, *Physical Review D* **92**, 123530 (2015).
  - [23] A. Szölgvény, M. MacLeod, and A. Loeb, *Monthly Notices of the Royal Astronomical Society* **513**, 54655473 (2022).
  - [24] D. O'Neill, D. J. D'Orazio, J. Samsing, and M. E. Pessah, *The Astrophysical Journal* **974**, 216 (2024).
  - [25] G. Chabrier, *Publications of the Astronomical Society of the Pacific* **115**, 763 (2003).
  - [26] D. C. Heggie, *Monthly Notices of the Royal Astronomical Society* **173**, 729 (1975).
  - [27] D. Raghavan, H. A. McAlister, T. J. Henry, D. W. Latham, G. W. Marcy, B. D. Mason, D. R. Gies, R. J. White, and T. A. ten Brummelaar, *The Astrophysical Journal Supplement Series* **190**, 142 (2010).
  - [28] J. D. Simon *et al.*, *The Astrophysical Journal* **976**, 256 (2024).
  - [29] J. Wolf, G. D. Martinez, J. S. Bullock, M. Kaplinghat, M. Geha, R. R. Muñoz, J. D. Simon, and F. F. Avedo, *Monthly Notices of the Royal Astronomical Society* **406**, 1220 (2010).
  - [30] Q. E. Minor, G. Martinez, J. Bullock, M. Kaplinghat, and R. Trainor, *The Astrophysical Journal* **721**, 11421157 (2010).
  - [31] C. Pianta, R. Capuzzo-Dolcetta, and G. Carraro, *The Astrophysical Journal* **939**, 3 (2022).
  - [32] A. Gratton, D. D. Hendriks, P. Das, D. Heber, and R. G. Izzard, *Monthly Notices of the Royal Astronomical Society* **543**, 1120 (2025).
  - [33] S. L. Splawaska, R. Errani, J. Peñarrubia, and M. G. Walker, arXiv preprint , arXiv:2602.11273 (2026).
  - [34] J. Peñarrubia, R. Errani, M. G. Walker, M. Gieles, and T. C. N. Boekholt, *Monthly Notices of the Royal Astronomical Society* **533**, 3263 (2024).
  - [35] J. Peñarrubia, R. Errani, E. Vitral, and M. G. Walker, arXiv preprint , arXiv:2506.03904 (2025).
  - [36] P. Gondolo and J. Silk, *Physical Review Letters* **83**, 1719 (1999).
  - [37] G. Bertone, A. R. A. C. Wierda, D. Gaggero, B. J. Kavanagh, M. Volonteri, and N. Yoshida, *Physical Review D* **112**, 043537 (2025).
  - [38] S. E. T. Smith *et al.*, *The Astrophysical Journal* **961**, 92 (2024).
  - [39] R. Errani, J. F. Navarro, S. E. T. Smith, and A. W. McConnachie, *The Astrophysical Journal* **965**, 20 (2024).

- [40] W. Cerny *et al.*, arXiv preprint , arXiv:2510.02431 (2025).
- [41] T. R. Adams, B. J. Brewer, and G. F. Lewis, *The Open Journal of Astrophysics* **9** (2026).
- [42] A. Drlica-Wagner *et al.*, *The Astrophysical Journal Supplement Series* **256**, 2 (2021).
- [43] B. Mutlu-Pakdil *et al.*, *The Astrophysical Journal* **918**, 88 (2021).
- [44] V. Manwadkar and A. V. Kravtsov, *Monthly Notices of the Royal Astronomical Society* **516**, 39443971 (2022).
- [45] K. Tsiane *et al.*, *The Open Journal of Astrophysics* **8**, 10.33232/001c.142072 (2025).
- [46] A. P. Cooper *et al.*, *The Astrophysical Journal* **947**, 37 (2023).
- [47] A. Skúladóttir *et al.*, *The Messenger* **190**, 19 (2023).
- [48] VIA Project, <https://via-project.org/>.
- [49] N. Esser, *Physical Review D* **112**, 043021 (2025).
- [50] R. Errani, J. Peñarrubia, and M. G. Walker, *The Astrophysical Journal* **993**, 160 (2025).

### Appendix A: Dimensionless functions

Here, we define all the dimensionless monotonic functions appearing in the main text.

The first such functions introduced are

$$\mathcal{A}(X) = \operatorname{erf}\left(\frac{X}{\sqrt{2}}\right) - \sqrt{\frac{2}{\pi}}X \exp\left(-\frac{X^2}{2}\right) \quad (\text{A1})$$

$$\mathcal{B}(X) = 3\mathcal{A}(X) - \sqrt{\frac{2}{\pi}}X^3 \exp\left(-\frac{X^2}{2}\right).$$

Taking the lower and upper limits of these functions, one finds  $\mathcal{A}(X \rightarrow 0) = \sqrt{2/\pi} X^3/3$ ,  $\mathcal{B}(X \rightarrow 0) = \sqrt{2/\pi} X^5/5$  and  $\mathcal{A}(X \rightarrow \infty) = \mathcal{B}(X \rightarrow \infty) = 1$ . Note that in the main text we use  $X \equiv v_i/\sigma$ , differing from Ref. [13], where  $X \equiv v_i/(\sqrt{2}\sigma)$  and  $\mathcal{A}(X)$  is redefined accordingly.

We also use

$$\mathcal{F}(e) = \frac{2 - e^2 - 2\sqrt{1 - e^2}}{e^2}, \quad (\text{A2})$$

which is such that  $F(0) = 0$  and  $F(1) = 1$ .

We finally introduce

$$\mathcal{K}(e, n) = \frac{(1 - e^2)^{\frac{n+3}{2}}}{2\pi} \int_0^{2\pi} \frac{(1 + e \cos \theta)^{-2}}{(1 + e^2 + 2e \cos \theta)^{n/2}} d\theta \quad (\text{A3})$$

which is such that  $\mathcal{K}(e, 3) > \mathcal{K}(e, 1)$ . It also satisfies  $\mathcal{K}(0, n) = 1$  and diverges as  $\mathcal{K}(e \rightarrow 1, n) \rightarrow \infty$ . In particular, carefully taking the limits of the integral yields in the zero-eccentricity limit

$$\lim_{e \rightarrow 0} \mathcal{K}(e, n) \simeq 1 + \frac{1}{4}n(2 + n)e^2, \quad (\text{A4})$$

while in the high-eccentricity limit

$$\begin{aligned} \lim_{e \rightarrow 1} \mathcal{K}(e, 1) &\simeq \frac{2}{\pi} \left[ -1 + \ln \left( \frac{8}{1 - e} \right) \right] \\ \lim_{e \rightarrow 1} \mathcal{K}(e, 3) &\simeq \frac{8}{\pi} \left( \frac{1}{1 - e} \right). \end{aligned} \quad (\text{A5})$$

The divergence of  $\mathcal{K}(e, 1)$  is logarithmic and therefore mild. Note that one must be cautious in the large- $e$  limit: Eq. (14), which makes use of  $\mathcal{K}(e, n)$ , eventually becomes non-physical because the apastron velocity becomes very small at high eccentricities, reaching  $\dot{x}|_{\text{apastron}} \lesssim v_{\text{cm}}$ , which contradicts the approximation used in the close binary case.

### Appendix B: Timescales comparison

Here, we compare the timescales associated with the effect of DM dynamical friction on the internal motion of wide binaries – e.g.,  $\tau_{w,1}$  (Eq. (9)) and  $\tau_{w,0}$  (Eq. (12)) – with those of other relevant mechanisms that may influence stellar dynamics in the typical UFD environments we consider, namely galactic tides, stellar encounters, and DM dynamical friction acting on the CoM of the pairs.

#### 1. Galactic tides

Galactic tidal forces induce a precession of the elliptic plane of binary systems, which may either compete with or act in concert with the effect of DM friction. The tidal potential of a binary in a host galaxy of mass  $M$  and radius  $\mathcal{R}$  is  $U_{\text{tide}} \sim GMa^2/\mathcal{R}^3$ . Comparing this with the two-body potential of the binary,  $U_{\text{pair}} \sim GM/a$ , gives a measure of the strength of the tidal perturbations. This strength is proportional to the ratio of the binary's internal orbital timescale to the tidal timescale, such that

$$\tau_{\text{tide}} \sim \frac{M}{\mathcal{M}} \left( \frac{\mathcal{R}}{a} \right)^3 \frac{2\pi a^{3/2}}{\sqrt{GM}} \sim 10^{10} \text{ yr} \left( \frac{10^3 \text{ AU}}{a} \right)^{3/2} \quad (\text{B1})$$

where the numerical estimate uses the DELVE 1 half-light radius and mass and assumes  $M = 2 M_{\odot}$ .

#### 2. Stellar encounters

Close encounters with passing stars can transfer momentum to binary systems, thereby altering their orbits. For wide binaries, stellar encounters can be treated using the impulse approximation [13], since the typical relative velocity between stars in UFDs,  $\sigma_{\text{rel}} \simeq \sqrt{2}\sigma$ , is much larger than the internal orbital velocity of such systems. The encounter rate of a binary with perturbers of impact parameter  $b$  is  $dN/dbdt = 2\pi b n_* \sigma_{\text{rel}}$ , where  $n_*$  is the local stellar number density. In the impulse regime, a single

fly-by of a perturbing star of mass  $m_p$  induces a change in the relative velocity of the binary components of order  $\Delta v \sim \pi G m_p / (b \sigma_{\text{rel}})$ , and therefore a (specific) energy kick  $\Delta E \sim \Delta v^2 / 2$ . The cumulative effect of multiple encounters leads to the rate  $\dot{E} = \int_{b_m}^{b_M} dN/dbdt \cdot \Delta E db$ , where  $b_m$  and  $b_M$  are the minimum and maximum impact parameters for weak impulsive encounters. Computing the integral leads to  $\dot{E} \sim \pi^3 n_* G^2 m_p^2 \ln \lambda / \sigma_{\text{rel}}$ , with  $\lambda = b_M / b_m$  [49]. A comparison with the binding energy of the pair gives the timescale

$$\tau_{\text{s.e.}} \sim \frac{8}{\pi^3 \ln \lambda} \frac{\sigma}{GM a n_*} \sim 10^{11} \text{ yr} \left( \frac{10^3 \text{ AU}}{a} \right), \quad (\text{B2})$$

where we set  $m_p = M/2$ . The numerical estimate assumes  $\ln \lambda = 2$ ,  $M = 2 M_\odot$ , and adopts the DELVE 1 velocity dispersion and stellar number density. The latter is estimated from the system's luminosity ( $M_V = -0.2$ ), implying it contains roughly 250 stars within its half-light radius, which corresponds to a density of  $n_* \simeq 0.1 \text{ pc}^{-3}$ .

### 3. Friction on the CoM

Another relevant timescale is the time taken by the pair to migrate towards the centre of the galaxy (or sink) due to dynamical friction acting on the centre-of-mass. Using  $\dot{E}_{\text{cm}} = \mathbf{f}_{\text{cm}} \cdot \mathbf{v}_{\text{cm}}$  (see Sec. II), one can derive the CoM energy loss rate in the limit of wide binaries. Comparing this with the CoM energy of the pair,  $E_{\text{cm}} \sim GMM/\mathcal{R}$ , yields the corresponding sinking timescale,

$$\tau_{\text{sink}} \sim \left[ \frac{4\pi G \rho_{\text{dm}} \mathcal{R} \ln \Lambda}{v_{\text{cm}}} \frac{(m_1^2 + m_2^2)}{MM} \mathcal{A} \left( \frac{v_{\text{cm}}}{\sigma} \right) \right]^{-1}. \quad (\text{B3})$$

For solar-mass stars with  $v_{\text{cm}} = \sigma$  in an environment typical of DELVE 1, one finds  $\tau_{\text{sink}} \sim 3 \times 10^9 \text{ yr}$ .

### 4. Comparison

In Fig. 4 we compare the various timescales described in the previous subsections with the wide binaries times-

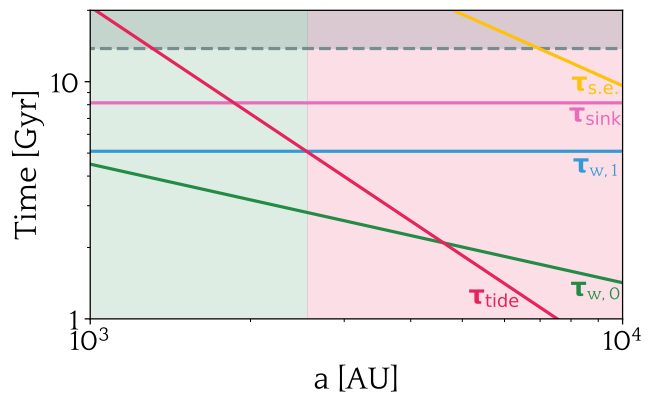


FIG. 4. Comparison of various dynamical timescales for wide binaries in an UFD galaxy. The upper grey region corresponds to times longer than the age of the Universe. The left green region indicates where DM dynamical friction dominates the long-term evolution of wide binaries. The right red region marks where at least one of the two wide-binary timescales exceeds the tidal timescale.

cales introduced in Eqs. (9) and (12), as a function of the semi-major axis  $a$ . As shown in the figure, galactic tides may dominate over internal DM friction in binaries wider than  $\sim 2000 \text{ AU}$ . They should therefore be carefully considered in any future, more detailed analysis of wide binary evolution in UFD galaxies.

Stellar encounters and dynamical friction on the centre-of-mass have timescales longer than  $\tau_{w,1}$  and  $\tau_{w,0}$ . Nevertheless, the sinking timescale of the binary pair as a whole remains shorter than the age of the Universe by a factor of a few, so stars are expected to migrate slightly toward the centres of UFDs. This mechanism could also potentially help constrain the DM content of faint galaxies, although it may be challenging due to the unknown formation sites of individual stars. Since the sinking time is also mass-dependent, it may lead to mass segregation and warrants further study (see also [50]).

Finally, note that we neglected any eccentricity dependence in all timescales, but a more careful analysis should account for it as well.